ACS APPLIED ENERGY MATERIALS

Open Access

This article is licensed under CC-BY 4.0

www.acsaem.org

Article

Ionomer Dispersions: Solvent Addition Sequence Matters

Marc Ayoub, Maximilian Wagner, Krishnaveni Anjala, Franziska Gröhn, Silke Christiansen, Jochen Kerres, Simon Thiele, and Matthew Brodt*

Cite This: ACS Appl. Energy Mater. 2025, 8, 9256−9267

Read Online

ACCESS | Metrics & More | Article Recommendations | Supporting Information

ABSTRACT: In this work we show that, when creating ionomer dispersions, in addition to the solvent composition, it is critically important to also consider the ionomer's solvent exposure history as this has an impact on its final dispersion state. By variation of the solvent addition sequence to the ionomer, the retainment of properties gained from previous solvent exposure states is illustrated. The order of solvent addition to the ionomer has a direct impact on the dispersions' final properties, such as the aggregate size and viscosity. Variations in dispersion properties subsequently affect catalyst inks, which in turn can lead to different coating qualities and distinct electrochemical behaviors. Notably, in fuel cell experiments, differences in the mass transport properties are observed, especially among electrodes with higher ionomer content, either due to different Knudsen diffusion processes in the catalyst layer or local O_2 diffusion through the ionomer films.

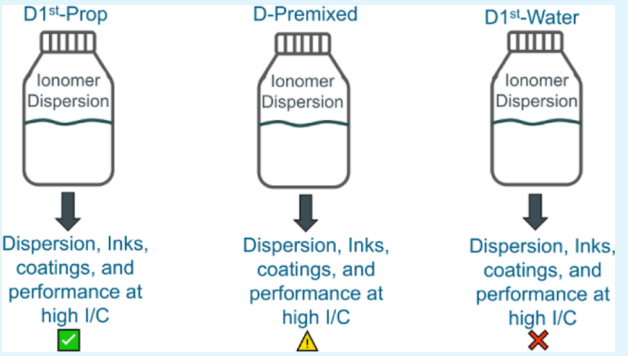

KEYWORDS: *ionomer dispersions, fuel cells, inhomogeneities, catalyst layers, coatings*

Downloaded via FORSCHUNGZENTRUM JUELICH on December 8, 2025 at 14:53:21 (UTC).
See https://pubs.acs.org/sharingguidelines for options on how to legitimately share published articles.

INTRODUCTION

Ionomer dispersions are fundamental for the fabrication of inks and electrodes in hydrogen-proton-exchange membrane fuel cells (H_2-PEMFCs). The ionomer is often based on perfluorosulfonic acid (PFSA) consisting of hydrophobic polytetrafluoroethylene backbones and hydrophilic sulfonic acid groups in their side chains. Commercially available ionomer dispersions can be purchased in different solid weight contents and usually contain alcohol and/or water as solvents.

Several studies have already investigated the influence of solvents on the morphology of ionomers in dispersions. Generally, it is understood that PFSA forms primary aggregates in the angstrom to nanometer range, the structure of which is dictated by the solvent environment. In colloidal and diluted systems with polar solvents, the primary aggregates have been reported to be rod-like.[1−4] The primary aggregates can form secondary aggregates (nanometers to a few μm), with the aggregate size and shape dependent on the solvent and ionomer concentrations. In one study, a 20 wt % ionomer dispersion was diluted to ≈3 wt % (1-propanol and ethanol) and rod-like shapes were found, which became smaller and thinner with increasing alcohol contents due to enhanced backbone solvation by alcohol.[5,6] A coarse-grained molecular dynamics (CG MD) simulation in dilute ethanol−water mixtures supported these findings up to ethanol concentrations of 50 wt %. At higher alcohol concentrations, the surface area and radius of gyration increased with the structure changing from cylindrical to solvated shapes as in experimental findings.[7−10] Another CG MD simulation showed an impact of the solid weight content, where higher 1-propanol concentrations resulted in smaller radii and longer aggregates for ionomer concentrations ≤5 wt %. However, for concentrations ≥7.5 wt %, both diameter and length increased for higher 1-propanol contents due to different electrostatic interaction strengths.[11] Through atomistic simulations of 29 wt % ionomer dispersions in low dielectric solvents, $\varepsilon \leq 45$ (ethanol, 2-propanol, glycerol, and toluene), physical cross-linking of the chains were observed.[12] These were driven by dominating attractive electrostatic interactions between $-SO_3^-$ and H_3O^+ ionic pairs resulting in loosely aggregated structures.[12] Higher dielectrics, however, can shield the ionic attractive charges of PFSAs causing less tightly bound chains and more dispersed backbones. Hence, for $\varepsilon \approx 56$ (formic acid), 2D lamellar-like aggregates were observed.[12] For higher values such as $\varepsilon \geq 78$ (water and formamide), the higher electrostatic shielding and lower backbone swelling result in dominant hydrophobic interactions between backbones. Such dielectric constants result in tightly packed elongated aggregates, which, in pure water, were cylinder-like.[12] Moreover, the radius of gyration, R_g, was smaller in water compared

Received: March 23, 2025
Revised: June 12, 2025
Accepted: June 13, 2025
Published: June 21, 2025

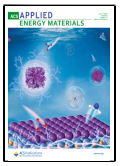

© 2025 The Authors. Published by American Chemical Society

to ethanol, 2-propanol, and glycerol, where R_g increased with aggregate swelling, as ϵ also increased.[12] This was similar to the correlation observed between solvent dielectric constants and solvent uptake of PFSA membranes by Kusoglu et al.[12,13]

The changes in morphology and structure also affect dispersions' viscosities. A CG MD simulation showed that viscosity measurements cause PFSA primary aggregates to break and transition into strands aligned in the sheared direction, resulting in shear thinning behavior.[14] For ≈4 wt % dispersions (equivalent weights (EWs) of dry polymer in grams per mole of SO_3 ≥ 1000 g mol^{-1}), the viscosities decreased with increasing alcohol contents.[1,15] On the other hand, for 4 wt % dispersions (EW 790 g mol^{-1}) in diacetone alcohol−water mixtures, and for solid contents ≥10 wt % in water−alcohol mixtures (various EWs), the viscosities increased with more alcohol.[16,17] These findings suggest that the complex interplay between molecular interactions and dispersion conditions is still not fully clear. Furthermore, influences of different ionomer morphologies on fuel cells and catalyst layers (CLs) are even less understood. One study found that diluting an ionomer dispersion (D79, 25 wt % in 99% water) with 1-propanol to ≈2.5 wt % followed by sonification promotes chain entanglement, which influences ink properties and ultimately fuel cell performance.[18] Expanding on previous findings, the current study aims to shed more light on the complex behavior of ionomers in dispersions. This is accomplished by varying the sequences of solvent addition to ionomers while examining how these lead to different dispersion characteristics, ink properties, coating qualities, and ultimately fuel cell performances. Consequently, pioneering efforts in this investigation illustrate how distinct microscopic properties due to varying processing parameters lead to different macroscopic outcomes. Ultimately, the complex nature of ionomers in dispersions and their impact on catalyst inks and fuel cells have been further elucidated.

EXPERIMENTAL SECTION

Dispersions. Small granule form short-sided chain (SSC) 3 M ionomer with an equivalent weight (EW) of ≈800 g mol^{-1} was used to prepare three different 20 wt % ionomer dispersions in water and 1-propanol mixtures. The final solvent mixtures consisted of 60 wt % anhydrous 1-propanol and 40 wt % Milli-Q water (18.2 MΩ·cm resistivity). For all dispersions, 2 g of ionomer was used in 100 mL of precleaned Schott bottles. The Schott bottles were placed on heating plates set at T = 80 °C corresponding to $T_{internal}$ ≈ 50 °C. Elliptical rare earth stirring bars (25 × 14 mm) were used to homogenize the dispersions at 500 rpm. For the first dispersion (D1st-Prop), the 1-propanol was pipetted in a Schott bottle, followed by the addition of the ionomer and a stirring bar. The heating plate was preset at 80 °C ($T_{internal}$ ≈ 50 °C) and the stirring speed to 500 rpm. The ionomer was allowed to swell for 2 h in 1-propanol, initially where some granules remained stuck at the glass interface before being integrated into a gel-like structure. After 2 h, the water was added to the mixture and left to homogenize over 3 days. After homogenization, the dispersion (D1st-Prop) was left to rest for 1 day. The second dispersion (D1st-Water) was prepared by first adding the water to the ionomer and allowing it to mix for 2 h on the heated plate at 500 rpm. Foams were observed, which after the addition of 1-propanol disappeared. Similarly, the dispersion (D1st-Water) was homogenized over 3 days with an extra day of resting. The third dispersion (D-Premixed) was prepared by first premixing the solvents and adding them together as a mixture to the ionomer. Similarly, as before, the dispersion (D-Premixed) was homogenized on the heated plate at 500 rpm over 3 days with an extra day of resting.

Catalyst Inks. All inks were prepared with a commercial Vulcan-based Pt/C catalyst (TEC10 V30E, ≈30 wt % Pt/C, Tanaka) first weighed (≈500 mg) in 15 mL HDPE bottles having ≈18 g of 5 mm ZrO_2 beads. Milli-Q water, 40 wt % (of total solvent content), was added to the catalyst first, and the HDPE bottle was then hand mixed. Afterward, the remaining 60 wt % of anhydrous 1-propanol was added followed by the prepared ionomer dispersion. The ionomer-to-carbon ratio (I/C) for the cathodes was 0.65 and 1.00, and the total solid weight content for each ink (i.e., catalyst and dry ionomer) was 10 wt %. As a result, six inks were made, two for each prepared dispersion. The I/C ratio for the anodes was 0.65, and the D1st-Prop dispersion was used for the anode ink. All inks were roller mixed at 60 rpm for ≈18 h at ≈22 °C.

Electrode and Cell Manufacturing. The inks were doctor-bladed at 100 mm s^{-1} (Proceq ZUA 2000.100) on virginal PTFE decal sheets (≈50 μm thick) placed on a coating table (COAT-MASTER 510, Erichsen) set at 60 °C with active vacuum at 30−40% relative humidity (RH). The wet film thickness for all inks was 300 μm, resulting in anode Pt loadings of 0.333 ± 0.031 mg cm^{-2}. The Pt loadings for the cathodes were, respectively, 0.350 ± 0.014 and 0.307 ± 0.025 mg cm^{-2} for the I/C ratio of 0.65 and 1.00. After drying, the electrodes were annealed at 180 °C for 10 min as per 3 M recommendation. Electrodes (5 cm^2) were stamped and hot pressed as in our previous study on 25 cm^2 GORE-SELECT membranes (M740.18; thickness 18 μm, W.L. Gore Associates) forming the catalyst coated membranes (CCMs).[19] The Pt loading was then determined gravimetrically by weighing the transferred decal sheet.

Ex Situ Analysis. Dynamic light experiments (DLS) were performed on the dispersions and inks by using a CGS 3 goniometer (ALV Langen, Germany) with a 22 mW laser with a wavelength of λ = 632.8 nm and an ALV 5000 correlator with 320 channels. The inks and dispersions were diluted 1:100 in 60 wt % 1-propanol and 40 wt % water mixtures. For better transparency of the ink solutions and to ensure accurate measurements, the inks were further diluted by 1:100. During the measurement, scattering angles of 30° ≤ θ ≤ 150° were covered in 10° steps. Data analysis of DLS was performed via transformation of the autocorrelation function of the scattered light intensity into the autocorrelation function of the electric field using the Siegert equation. A regularized inverse Laplace transformation was carried out with the program CONTIN. The diffusion coefficient, D (q = 0), was obtained by extrapolation and used for the determination of the hydrodynamic radii, R_H, via the Stokes−Einstein equation.

For viscosity measurements, the HDPE bottles containing the inks were first allowed to rest for ≈5 min. 500 μL of the samples was slowly pipetted onto a HAAKE MARS 40 Rheometer with a C60 0.5°/Ti cone at 20 °C. No bubbles were observed during the pipetting process, and each measurement was repeated three times. The viscosity was linearly screened in 40 steps between shear rates of 10 and 400 s^{-1}, while holding each step for 10 s to reach a steady state response. After the steady state response, the viscosity was acquired over 3 s (total hold time 13 s per step). Oscillatory amplitude sweep (OAS) measurements were performed as well, at least twice for each sample, and the average of the min−max deviation is reported. First, the sample was pre-sheared for 30 at 200 s^{-1}, and then a strain of 0.01% was applied at 1 Hz for 60 s. OAS measurements were performed from 0.01% to ≈12% at 1 Hz and with 22 steps. The sample was afterward sheared again for 30 at 200 s^{-1}.

The contact angles of the inks were measured using a DSA 30 drop shape analyzer from Krüss using their ADVANCE software. The measurements were done using the sessile drop method, an automatic baseline detection method, and an automatic tangent fit method for the left and right contact angles. The tests were done on virginal decal sheets for two min while taking a measurement every 30 s. The angles reported are the averages of the left and right contact angles.

To get an idea of the coating qualities, the decal coated sheets were placed on a Dörr LT-2020 LED lightning tablet set at a maximum white lighting for imaging. Pictures were then taken at a fixed distance using a Canon EOS 6D camera with ISO set to Auto, a shutter speed of 1:4000, an aperture of F/2.8, and a Tamron SP 90 mm F/2.8 Ø58 Macro 1:1 VC USD objective/lens. For a more comprehensive and complete analysis, scanning electron microscopy (SEM) imaging was

https://doi.org/10.1021/acsaem.5c00850
ACS Appl. Energy Mater. 2025, 8, 9256−9267

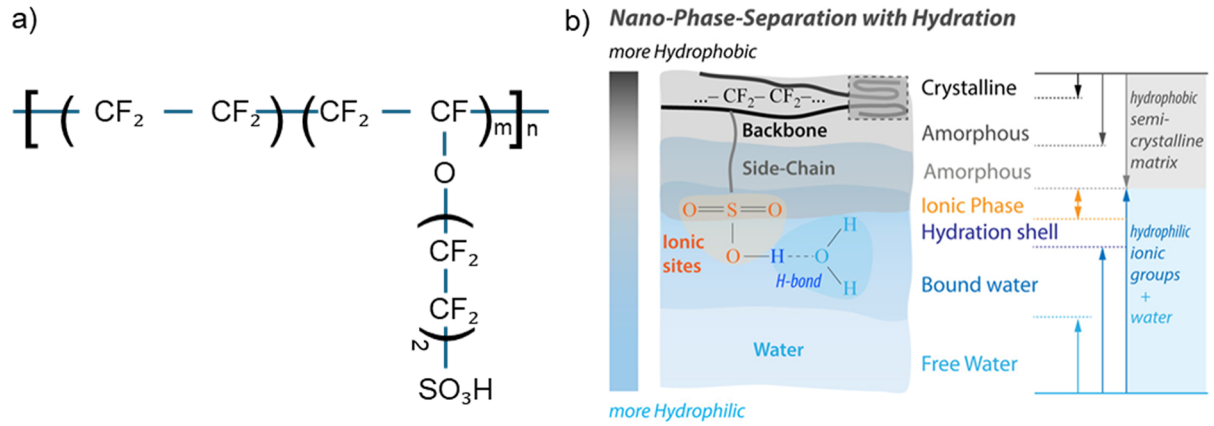

Figure 1. Properties of the SSC 3 M ionomer with an EW of 800 g mol^{-1} used in this study with (a) showing its chemical formula. The number of tetrafluoroethylene repeating units is given by *m* and the number of block repetitions by *n*. (b) shows the amphiphilic distribution of the ionomer, along with some common properties for PFSA ionomers. (b) is adapted and reprinted with permission from Kusoglu et al.[13] Copyright 2017, American Chemical Society.

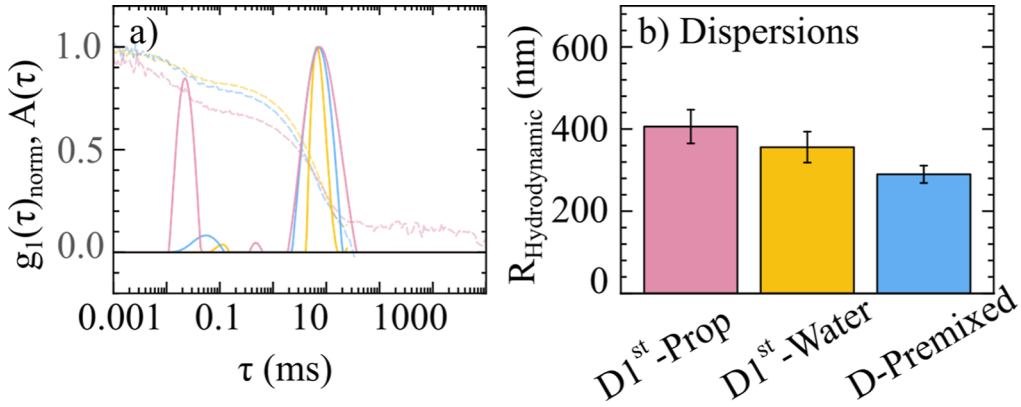

Figure 2. a) Intensity distribution functions of the scattered light A(τ) for D1st-Prop (pink —), D1st-Water (yellow —), and D-Premixed (blue —) with the autocorrelation functions of the electric field $g_1(\tau)$ (same colors, dashed lines) at 90° angle; (b) calculated hydrodynamic radii, R_H, using Stokes−Einstein equation based on angular extrapolated data. The first peak for D1st-Prop (pink —) was around 0.81 ± 0.09 nm, and the second peak 406 ± 41 nm. The radii in (b) are for the second peaks.

done on cross-sectionally embedded membrane electrode assemblies (MEAs) as in our previous study.[19]

Electrochemical Analysis. Three MEAs for each I/C ratio per dispersion were tested using an automated protocol between a commercial 850e FC testing system (Scribner Associates, Inc.) and a VSP-300 potentiostat (BioLogic). Commercial gas diffusion layers were used for the anodes and cathodes (5 cm^2 H14CX483, Freudenberg) compressed by 25 ± 1% using glass-fiber-reinforced PTFE gaskets. A commercial 5 cm^2 cell fixture was used with a torque of 5 N m as reported previously.[19]

Cell tests started with linear sweep measurements under fully humidified conditions at 80 °C and 150 kPa absolute and atmospheric pressure with 0.20 L min^{-1} H_2 on the anode and 0.20 L min^{-1} N_2 on the cathode. Shorts were checked with a scan rate of 2 mV s^{-1} from ≈0.1 to 0.4 V.[20,21]

Cells were then broken-in by voltage cycling 7−10 times between 0.6 V (20 min hold) and 0.3 V (20 min hold) with open circuit voltage (OCV) periods (2 min) in between.[22] The flow rates at 94% RH (dew point = 78.5 °C) and 150 kPa absolute pressure were 0.20 L min^{-1} H_2 on the anode and 0.75 L min^{-1} air on the cathode. Afterward, polarization curve measurements were performed in galvanostatic mode with 10 steps between 0 and 0.100 A cm^{-2} and 13 steps between 0.150 A cm^{-2} and 2.200 A cm^{-2}. The hold time was 2.5 min for each step of which the last 30 s were averaged for the voltage response. Then galvanostatic impedance spectroscopy measurements were done to obtain the high frequency resistances (HFR). The measurements were done at each step with a 10% amplitude, 10 points per decade, 2−3 average measures per frequency, and from 500 kHz to at least 0.4 Hz. The highest frequency for analysis was limited to 30 kHz due to higher noise at higher frequencies.

The protonic sheet resistance of the CL based on 6 measurements was quantified for one representative MEA for each I/C ratio per dispersion. The anodes and cathodes had, respectively, flow rates of 0.20 L min^{-1} of H_2 and N_2 at 94% RH %, 80 °C, and atmospheric pressure. The impedance measurement was performed at 0.2 V potentiostatically with an amplitude of 10 mV from 500 kHz to 0.2 Hz, with 10 points per decade, and 5 average measurements per frequency. As before, the highest frequency for analysis was limited to 30 kHz. The impedance spectra were fitted using the "Z-Fit" function in EC-Lab software with the "Randomize + Simplex" method.[23−25] Having determined the crossover, HFR, and protonic sheet resistance, the Tafel slope for the samples was calculated for the IR_{free} plot in the linear region until 0.100 A cm^{-2}.

Limiting current experiments were performed at atmospheric, 150, 200, and 300 kPa absolute pressures using oxygen concentrations of 3 vol %, 3.5 vol %, 4 vol %, and 5 vol % in N_2 (0.95 L min^{-1} total flow rate) on the cathode and 0.20 L min^{-1} of only H_2 on the anode. The limiting current was measured potentiostatically from 0.5 to 0.1 V (ΔV = 0.1 V) and then from 0.07 to 0.05 V (ΔV = 0.01 V). Each step was held for 1 min of which the last 30 s were averaged. The limiting currents were determined to have been reached at 0.07 V, and the mass transport resistances were compared at 30% RH, ensuring minimal flooding conditions. The mass transport resistance R_{T,O_2} was

https://doi.org/10.1021/acsaem.5c00850
ACS Appl. Energy Mater. 2025, 8, 9256−9267

determined and deconvoluted into pressure dependent, R_{PD,O_2}, and pressure independent, R_{PI,O_2}, components using the method described by Baker et al., $R_{T,O_2} = R_{PD,O_2} + R_{PI,O_2}$.[26]

To visualize key differences and features among the samples better, the aforementioned electrochemical analysis (excluding LSV) was performed not only at 94% RH but also at 30% RH and 15% RH under symmetric conditions. To recondition the cells to the different operating conditions, short voltage cycles 4−5 times between 0.6 V (5 min hold) and 0.3 V (5 min hold) with the OCV in between (30 s) were performed initially.

Finally, three cyclic voltammetry measurements were performed to estimate the electrochemical active surface area (ECSA, $m^2 g_{pt}$). The scan rate used for analysis was 100 mV s^{-1}, and the voltage was screened between 0.03 and 0.6 V at 40 °C, 100% RH, and atmospheric pressure. Five percent H_2 in N_2 was supplied on the anode at 0.50 L min^{-1}, while the flow rate on the cathode was set to 0 after purging N_2. The q_{HUPD} region was integrated for ECSA calculation between 0.06 and 0.40 V, assuming an adsorption charge of 210 μC cm^{-2} for Pt.[21]

RESULTS AND DISCUSSION

Dispersion Properties. A depiction of the chemical formula of the ionomer used in this study is given in Figure 1a. It shows the hydrophobic backbone and the hydrophilic sulfonic acid of the side chain. A distribution of the amphiphilic behavior within the nanophase-separated structure is also shown in Figure 1b. Since the first-added solvent (and thus the solvent polarity) was varied in this investigation, differences in the initial affinity for hydrophobic and hydrophilic ionomer−solvent interactions are expected. This is also reflected in the DLS results.

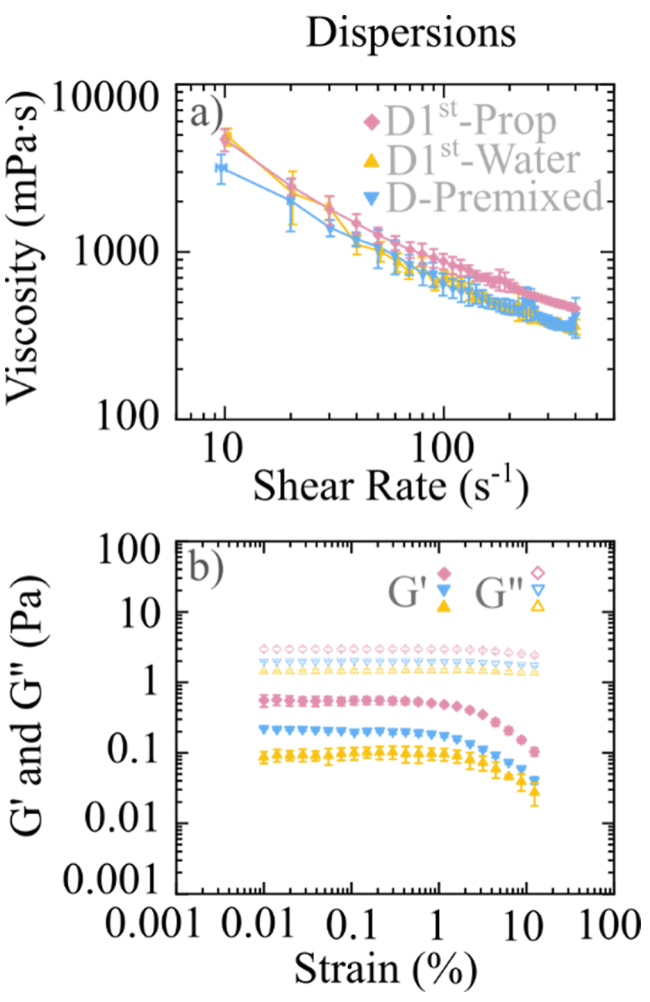

Figure 3. a) Viscosity measurements for the different dispersions, D1st-Prop (pink −♦−), D1st-Water (yellow −▲−), and D-Premixed (blue −▼−) repeated each three times. (b) OAS measurements of the dispersions measured at least twice.

Before diving into the DLS data, abbreviations with their colors are introduced for the differently prepared samples: (i) ionomer dispersions where 1-propanol was first added to the ionomer before the addition of water are referred to as D1st-Prop (pink —). (ii) Dispersions where water was added before 1-propanol are referred to as D1st-Water (yellow —). (iii) Finally, dispersions prepared by first premixing the solvents and then adding them together as a mixture to the ionomer are referred to as D-Premixed (blue —).

During the preparation of the ionomer dispersions, the formation of a gel-like structure was observed for the D1st-Prop dispersion before the addition of water. Both the D1st-Water and D-Premixed dispersions did not show the formation of a gel-like structure. However, the D1st-Water dispersion showed heavy foam formation before the addition of 1-propanol. In the DLS results in Figure 2a, the first peak, at low decay times (τ), is strongly visible for D1st-Prop, whereas the second peak is between $1 < \tau < 30$ ms, similar as for other dispersions. More exposure to water in the beginning of the dispersion preparation led to the decrease of the first peak for D-Premixed (blue —) and D1st-Water (yellow —). The first peaks close to $\tau = 0.1$ ms are likely 1-propanol associates with a size of roughly $R_H = 0.9$ nm (determined for sample D1st-Prop).[27] At high decay times close to $\tau = 1000$ ms, the baseline for D1st-Prop (pink ---) stayed above 0 indicating slow diffusion, which might be caused by the presence of larger particles or a more interconnected network. For the other samples, the baseline approached zero (Figure S4). Treating the ionomer with high alcohol contents has been shown to result in highly solvated aggregates,[7,8,10,12,17] where dominant electrostatic interactions between ion pairs ($-SO_3^-$ and H_3O^+) lead to chain clustering, which in turn can prevent dissolution despite high backbone swelling, as in.[28] The experimental observation of a gel-like structure in 1-propanol + PFSA (first 2 h of D1st-Prop preparation) supports this phenomenon. However, the consistency of the gel-like structure is not known, with potentially different cluster sizes forming. This could also explain the higher baseline for D1st-Prop (pink —) close to $\tau = 1000$ ms, Figure 2a.

The peaks around $1 < \tau < 30$ ms show a broader distribution successively for D1st-Water (yellow —), D-Premixed (blue —), and D1st-Prop (pink —). The broader peak indicates the existence of a wider cluster size distribution for D1st-Prop (pink —), whereas anisotropic interactions could have led to an intermediate distribution for D-Premixed (blue —). In contrast, less chain clustering initially could have led to the smallest distribution for D1st-Water (yellow —). Calculated radii in Figure 2b between $1 < \tau < 30$ ms resulted in the largest R_H (406 ± 41 nm) for the D1st-Prop dispersion (pink —), followed by intermediate sizes (356 ± 38 nm) for D1st-Water (yellow —), and the smallest size (290 ± 21 nm) for D-Premixed (blue —). It has been reported that high solid weight content dispersions with high water content have smaller radii than dispersions with more alcohol.[11,12,17] A similar behavior is witnessed here despite the dispersions having the same final overall compositions. The addition of

https://doi.org/10.1021/acsaem.5c00850
ACS Appl. Energy Mater. 2025, 8, 9256−9267

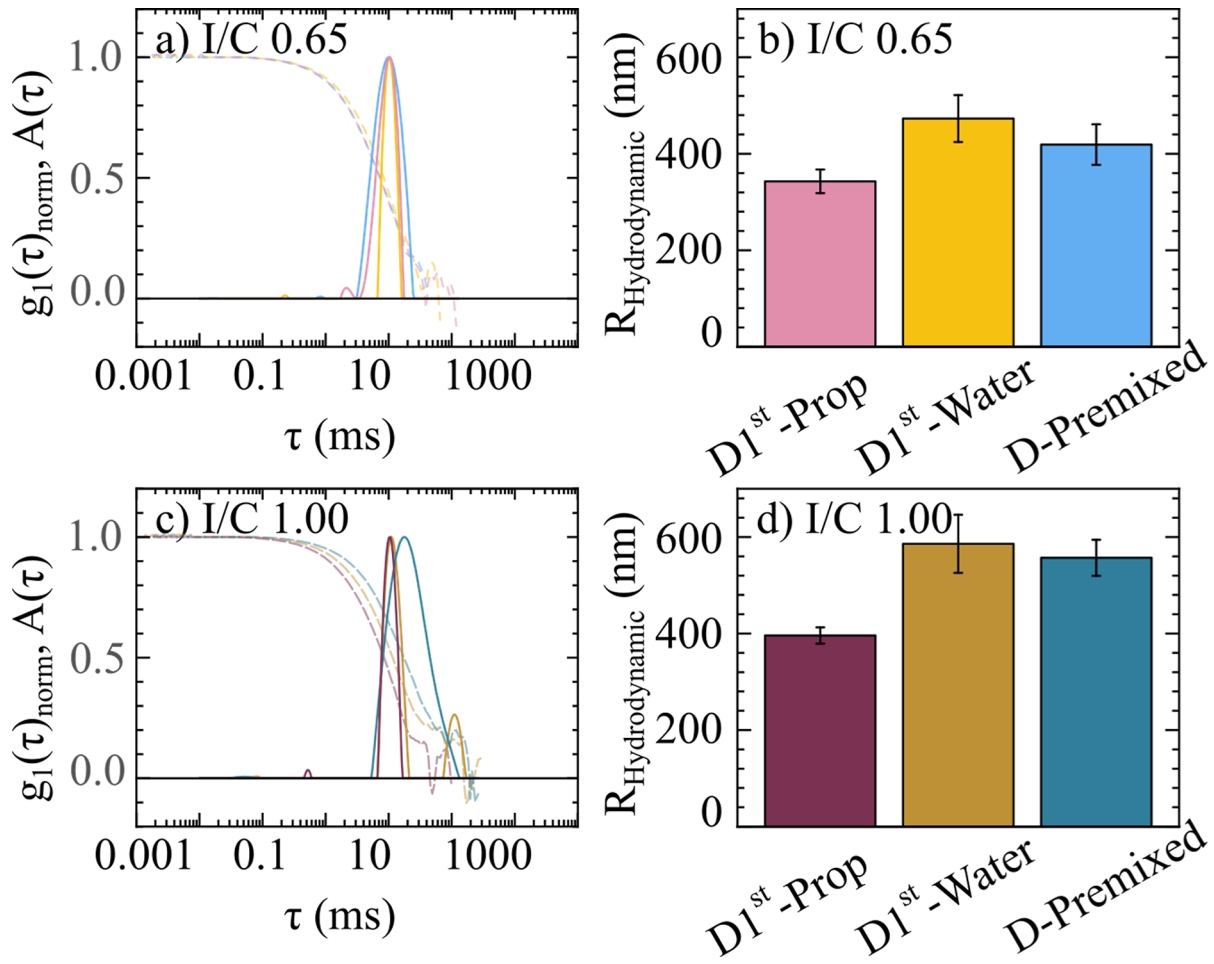

Figure 4. Intensity distribution functions of the scattered light A(τ) for an I/C ratio of (a) D1st-Prop (pink —), D1st-Water (yellow —), and D-Premixed (blue —) with the autocorrelation functions of the electric field $g_1(\tau)$ (same colors, dashed lines) at 90° angle; (b) calculated hydrodynamic radii for an I/C ratio of 0.65. (c) Intensity distribution functions of the scattered light A(τ) for an I/C ratio of 1.00 D1st-Prop (brown —), D1st-Water (dark yellow —), and D-Premixed (teal —) with the autocorrelation functions of the electric field $g_1(\tau)$ (same colors, dashed lines) at 90° angle; (d) calculated hydrodynamic radii, R_H, using Stokes−Einstein equation for an I/C ratio of 1.00.

water first to the ionomer in D1st-Water (yellow —) reduced ionic clustering, as in an atomistic simulation study and a membrane simulation study.[12,29] The hydrophobic effect leading to tightly packed backbones is enhanced in that scenario, likely resulting in elongated cylindrical structures as reported in various experiments.[3,6,12,30,31] For D1st-Prop (pink —), electrostatic ionic attractions are initially dominant, causing more chain clustering. After the addition of the second solvent, the ionomer is prone to shift to another state yet maintains some properties from their previous water- or alcohol-rich state. These initial properties resulted in the different aggregate sizes among the dispersion variations, despite the dispersions having the same overall final composition. The above observations suggest that the solvent history and solvent addition sequence to the ionomer matter. The D-Premixed (blue —) dispersion can in theory be prone to anisotropic effects due to localized hydrophobic and ionic clusters forming during the preparation. However, since the ionomer is directly exposed to the mixture, extreme aggregation effects due to hydrophobic interactions of the backbones and ionic clustering of the side chains are lowered. Ultimately, avoiding the extreme clustering effects could have led to a more readily dissolved state with the smallest R_H value in Figure 2b.

Viscosity measurements in Figure 3a indicate a higher viscosity for D1st-Prop (pink −◆−) at high shear rates than for D1st-Water (yellow −▲−) and D-Premixed (blue −▼−). At low shear rates, the deviation between repetitions prevents precise interpretation of the thinning behavior. The D-Premixed (blue −▼−) dispersion shows deviations encompassing both other dispersions, indicating more dispersion inhomogeneity. The origin of the inhomogeneity could be due to some anisotropic effects of localized hydrophobic and ionic clustering during dispersion preparation before completely dissolving. However, the exact reason remains unknown. OAS measurements, Figure 3b, reveal a high increase in storage modulus related to the solid-like behavior of the dispersions, G', and a small increase in the loss modulus related to the fluid-like behavior of the dispersions, G'', for samples more initially exposed to 1-propanol during preparation before the addition of water. As a result, G' and G'' were highest for D1st-Prop (pink —), followed by D-Premixed (blue −▼−), and then by D1st-Water (yellow −▲−). Furthermore, all dispersions showed dominant viscous (fluid-like) behavior since G'' was bigger than G'. The observed differences among the dispersions suggest different viscoelastic properties for the samples. The more pronounced increase in G' for D1st-Prop (pink —) compared with D1st-Water

https://doi.org/10.1021/acsaem.5c00850
ACS Appl. Energy Mater. 2025, 8, 9256−9267

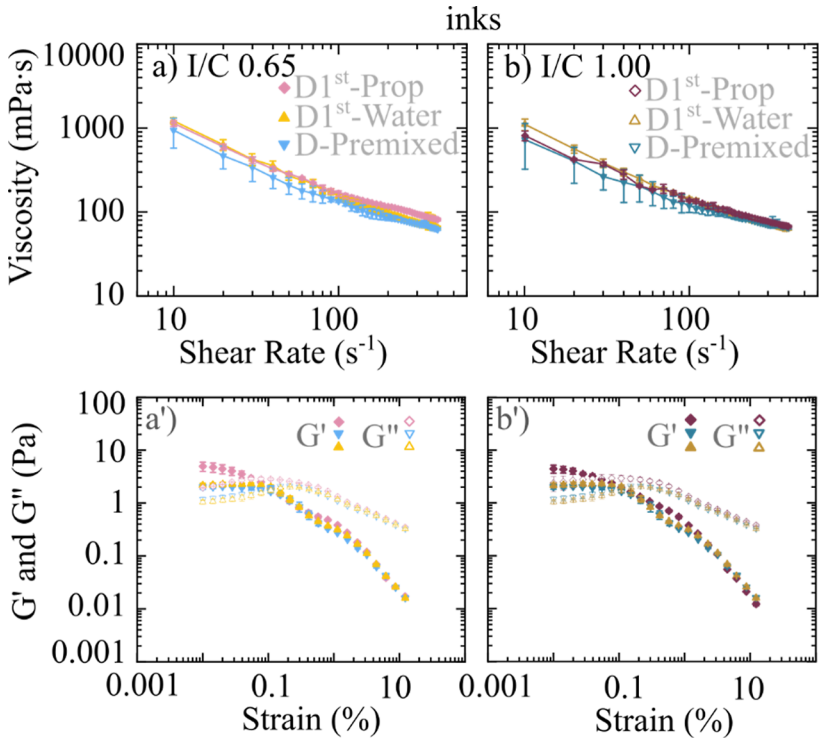

Figure 5. Viscosities for different inks repeated three times each, (a) I/C ratio 0.65, D1st-Prop (pink −♦−), D1st-Water (yellow −▲−), and D-Premixed (blue −▼−); (b) I/C ratio 1.00 D1st-Prop (brown −◊−), D1st-Water (dark yellow −△−), and D-Premixed (teal −▽−). (a') and (b') are the respective OAS measurements of the inks with I/C 0.65 and I/C 1.00.

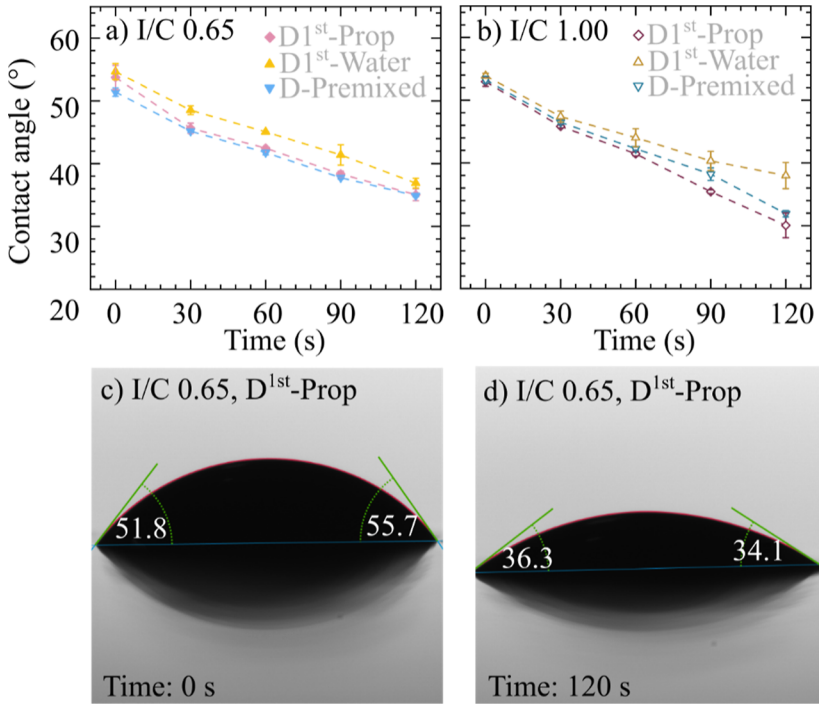

Figure 6. a) Contact angle values for an I/C ratio of 0.65, D1st-Prop (pink −♦−), D1st-Water (yellow −▲−), and D-Premixed (blue −▼−); (b) an I/C ratio of 1.00, D1st-Prop (brown −◊−), D1st-Water (dark yellow −△−), and D-Premixed (teal −▽−). (c) and (d) show contact angle measurements for an I/C ratio of 0.65, D1st-Prop (pink −♦−) at 0 s and after 120 s.

(yellow −▲−) suggests a more physically connected domain with stronger interchain or interparticle associations that resist deformation. As a matter of fact, an experimental study reported higher viscosities for higher alcohol and solid weight contents due to enhanced interaggregate associations.[17] However, all samples started deforming at similar strain values, indicating that the yield point remains unaffected. This suggests that the underlying structural architecture is unchanged, while the magnitudes of interaction strengths change due to the different viscoelastic properties.

https://doi.org/10.1021/acsaem.5c00850
ACS Appl. Energy Mater. 2025, 8, 9256−9267

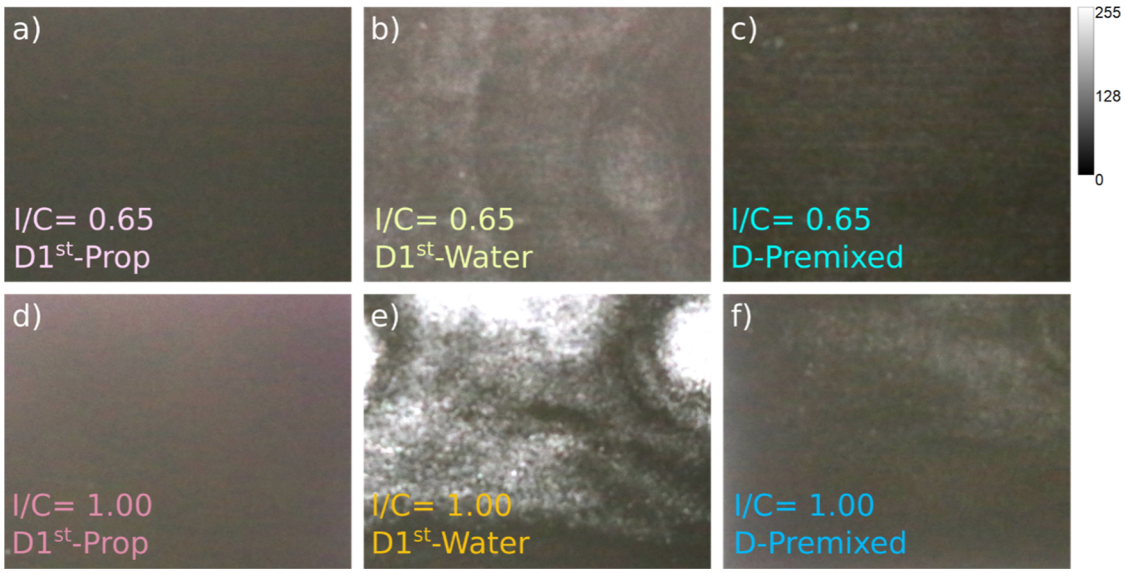

Figure 7. Coating qualities of the different inks (a–f) with a Canon EOS 6D camera, Auto ISO, and a shutter speed of 1:4000, processed with ImageJ with a maximum value of 120 in Brightness/Contrast tool. The scalebar depicts the maximum brightness value.

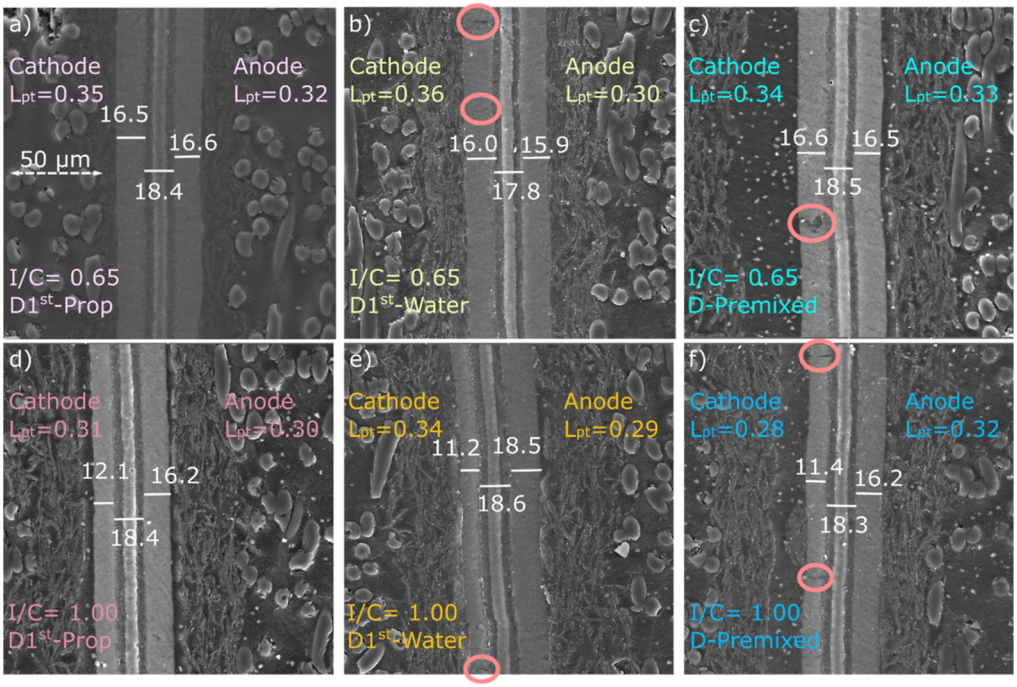

Figure 8. Images (a–f) were taken at 20.0 kV, a working distance of 5 mm, and a view field of 200 μm. Platinum loadings are given in the top of each image (in mg_{Pt} cm^{-2}), and thicknesses are given in the center of the images (in μm). Formed inhomogeneities are marked with a light red circle.

To confirm the trends observed in the DLS and rheological measurements, ionomer dispersions with 9 wt % solid content were also prepared using the same method described in the experimental section. The initial observations remained similar, with D1st-Prop forming a swollen structure before the addition of water, D1st-Water forming a foam before the addition of 1-propanol, and D-Premixed showing none of the previous behaviors. Also, similar observations were made when the rheological and DLS data of D1st-Prop were compared to those of the remaining samples (Figures S6 and S7). However, the DLS and rheological data for D1st-Water and D-Premixed were within the error bars. This can be due to several reasons, such as nonideal mixing of the solvents before addition to the ionomer in the D-Premixed dispersion, and/or different degrees of anisotropy for the less diluted mixture.

Ink Properties. The 20 wt % ionomer dispersions were mixed with catalyst and additional solvent to make catalyst inks, which were also analyzed using DLS and viscosity measurements. The dispersions were combined with catalysts at two different ionomer-to-carbon ratios (I/C) while maintaining the same overall solvent compositions as those in the dispersions. Figure 4a,b shows the DLS results and the resulting R_H, respectively, for the different dispersions with I/Cs of 0.65. Contrary to the dispersion results, the inks showed

https://doi.org/10.1021/acsaem.5c00850
ACS Appl. Energy Mater. 2025, 8, 9256–9267

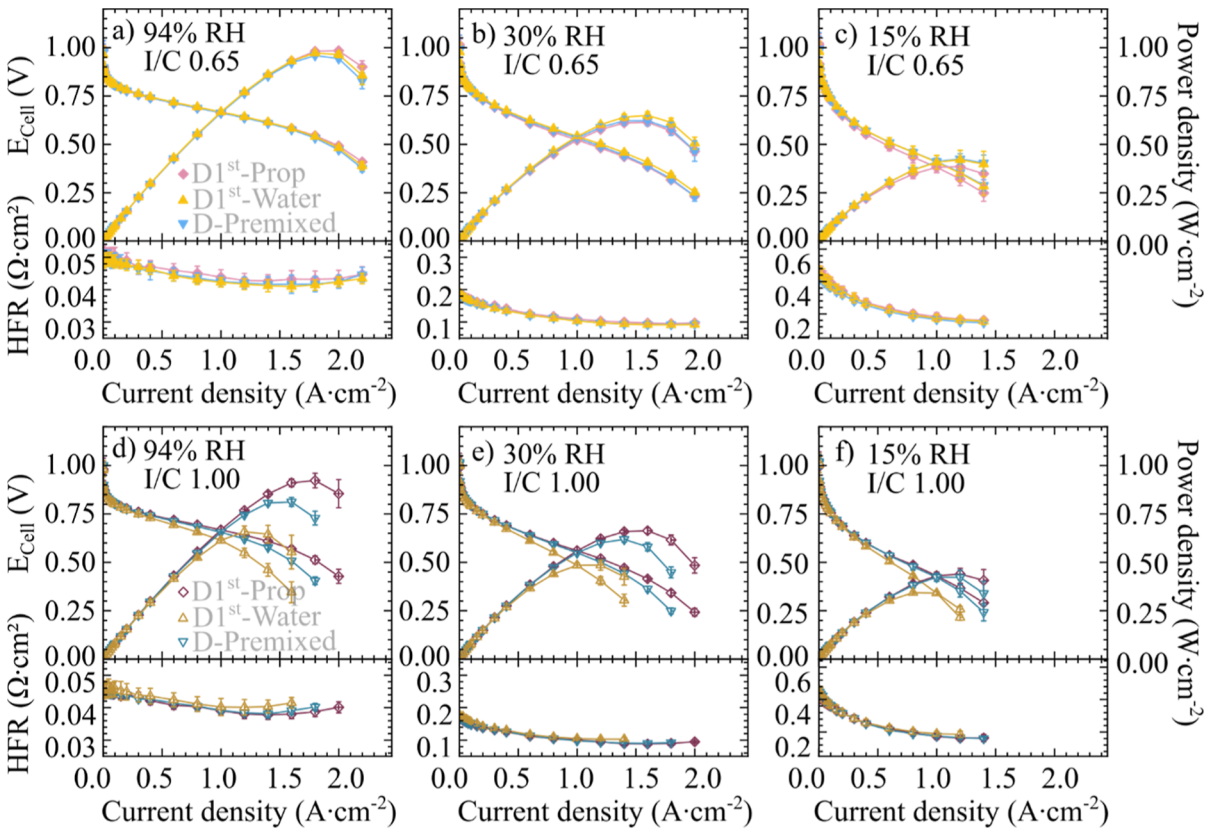

Figure 9. Averaged performance curves and HFRs based on three measurements with 0.2 L min^{-1} H_2 on the anode and 0.75 L min^{-1} air on the cathode at 80 °C and 50 kPa gauge backpressure for an I/C ratio of 0.65, D1st-Prop (pink −♦−), D1st-Water (yellow −▲−), and D-Premixed (blue −▼−) at (a) 94% RH, (b) 30% RH, and (c) 15% RH, and for an I/C ratio of 1.00, D1st-Prop (brown −◊−), D1st-Water (dark yellow −△−), and D-Premixed (teal −▽−) at (d) 94% RH, (e) 30% RH, and (f) 15% RH.

monodisperse samples with peaks between $1 < \tau < 30$ ms regardless of the dispersion preparation method. This was also the scenario for I/Cs of 1.00 for the different dispersions, as shown in Figure 4c,d.

Obtained values for R_H (from about 340 to about 590 nm) of the inks (Figure 4) showed different trends with respect to the solvent addition order as compared to the ionomer dispersions without catalyst. However, each of the inks with the higher I/C ratio had a higher R_H value in comparison to the ink with the lower I/C value made from the same ionomer dispersion, suggesting more ionomer covering of the catalysts. Regardless of the I/C ratio, inks with D1st-Prop dispersions (pink — or brown —) always had the smallest radii, whereas D1st-Water inks (yellow — or dark yellow —) always had the largest radii, and D-Premixed inks (blue — or teal —) showed values in between. The smaller radii of the ink from the D1st-Prop dispersion may originate from a higher interaction with the hydrophobic catalyst; the D1st-Prop had higher viscosities and bigger aggregates and retained a more hydrophobically swollen structure. The polydisperse behavior observed for the D1st-Prop dispersion (Figure 2a) may result in small particles filling voids between larger aggregates, which could lead to better homogenization during the roll milling process. A similar explanation was also provided in[18] where similar results were observed. The D1st-Water dispersion had the lowest R_H and viscosities, exhibiting less structure swelling, association, and likely more packed backbones as reported from literature in pure water.[12] As a result, hydrophobic ionomer−catalyst interactions are less favorable, leading to less ink homogenization and aggregate size reduction. For the inks made with the D-Premixed dispersion, anisotropy in the original mixture could have led to partial localized hydrophobic and ionic clusters during the preparation. Thus, the overall ionomer−catalyst interaction strengths were in between those of D1st-Prop and D1st-Water, which in turn led to intermediate R_H values. These observations are further supported by different coating qualities, which are discussed later.

Viscosity measurements of inks in Figure 5a show that the I/C 0.65 D1st-Prop (pink −♦−) ink had the highest viscosity at high shear rates (the relevant coating region). Interestingly, Figure 5b shows almost overlapping viscosities for the inks with an I/C ratio of 1.00 regardless of the ionomer dispersion preparation method. These are slightly lower than the viscosities of I/C 0.65 D1st-Water (yellow −▲−) and I/C 0.65 D-Premixed (blue −▼−). Higher ionomer content for the I/C ratio of 1.00 leads to a higher ionomer saturation in the ink, compared with I/C 0.65. As a result, more ionomer adsorption on the catalyst enhances electrostatic repulsion lowering carbon−carbon attraction and leads to lower viscosities than the lower I/C of 0.65.[32,33] To visualize possible differences better, corresponding OAS measurements were made, Figure 5a',b'. These show a predominately elastic behavior at low strain ($G' > G''$) within the linear viscoelastic region for all inks, which at higher strain transition into a fluid-like viscous dominant behavior, ($G'' > G'$). At low strain, the D1st-Prop inks displayed consistent higher values in G' than the remaining inks, suggesting possibly enhanced ionomer−catalyst and ionomer−ionomer interaction strengths. At higher

https://doi.org/10.1021/acsaem.5c00850
ACS Appl. Energy Mater. 2025, 8, 9256−9267

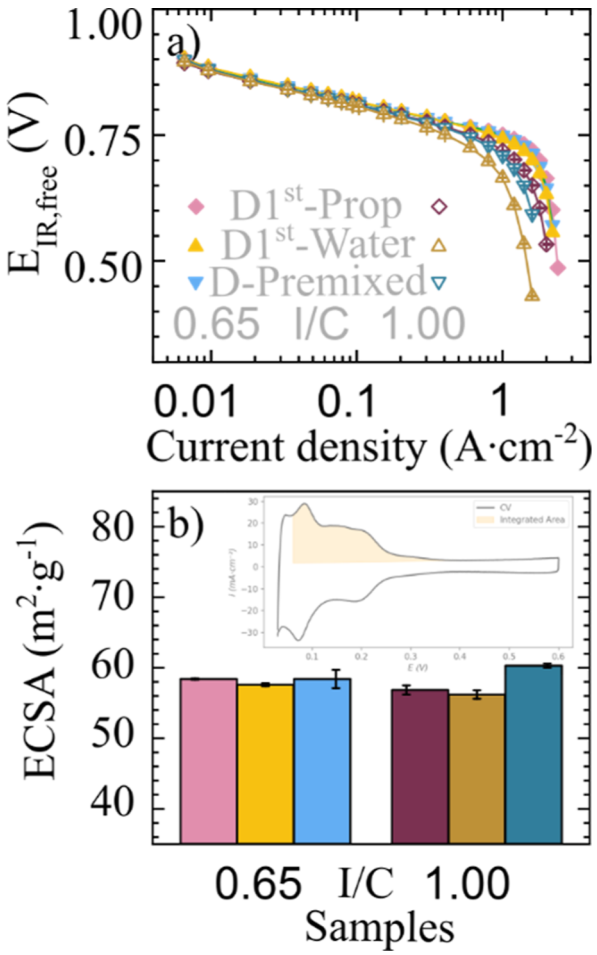

Figure 10. Comparisons of ECSAs and Tafel slopes for I/Cs 0.65 D1st-Prop (pink −♦−), D1st-Water (yellow −▲−), and D-Premixed (blue −▼−) and 1.00 D1st-Prop (brown −◊−), D1st-Water (dark yellow −△−), and D-Premixed (teal −▽−) for (a) averaged Tafel slopes, corrected for the crossover, HFR, and protonic sheet resistance, calculated at 80 °C, 50 kPa gauge backpressure, and 94% RH. (b) ECSAs calculated at 40 °C, atmospheric pressure, and 100% RH.

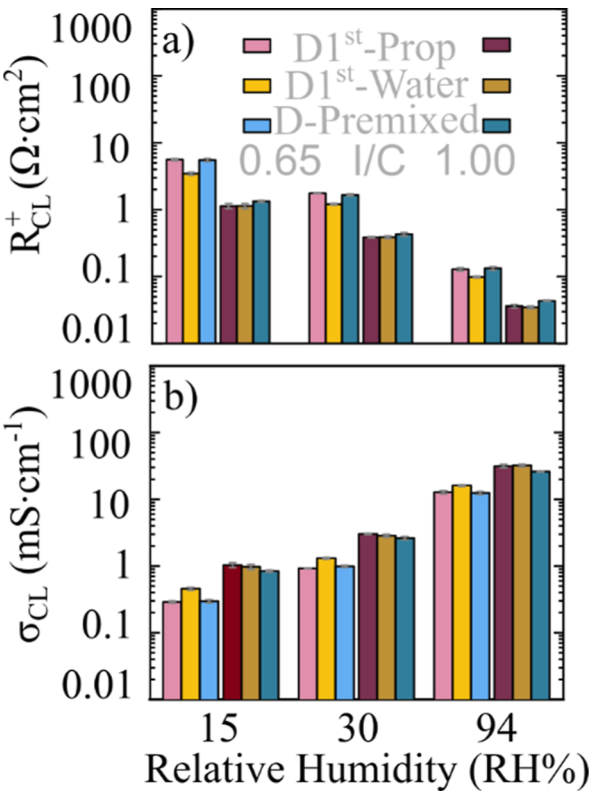

Figure 11. Impedance measurement results under blocking conditions at 0.2 V displaying the (a) proton sheet resistance at different RHs. (b) Conductivity values normalized to the CL thickness at different RHs for 0.65 D1st-Prop (pink —), D1st-Water (yellow —), and D-Premixed (blue —) and I/Cs 1.00 D1st-Prop (brown —), D1st-Water (dark yellow —), and D-Premixed (teal —).

strains, these differences disappear, with G' and G'' showing similar responses for all inks. Furthermore, the inks with the D-Premixed and D1st-Water dispersions showed similar behaviors for all strains, suggesting no considerable differences.

Contact Angle Measurements. Figure 6a,b shows the contact angles of the inks with I/Cs of 0.65 and 1.00, respectively. For both I/C ratios, a continuous decrease of the contact angle was observed with time. Furthermore, worse wetting properties were observed for both I/C ratios for the inks prepared with D1st-Water (yellow — or dark yellow —) as time elapsed. The inks with the D-Premixed (blue — or teal —) and D1st-Prop dispersions (pink — or brown —) had overall better wetting behaviors, with the ink of I/C 1.00 D1st-Prop (brown −◊−) being slightly better than the ink of I/C 1.00 D-Premixed (teal −▽−). These observations suggest that the dispersions first exposed to 1-Propanol during preparation result in inks with more favored hydrophobic interactions and, consequently, better wetting behaviors.

Coating Qualities. The different degrees of ink-wetting from the contact angle measurements are also reflected in the coating qualities. For a better illustration, the camera images were processed with a simple adjustment of the maximum display value in the Brightness/Contrast tool within the ImageJ software to enhance the visibility of surface inhomogeneities. The value for maximum was lowered to 120 for all images, effectively enhancing the contrast in dark regions. The original images can be found in the Supporting Information (Figure S1).

Figure 7 clearly shows that the different preparation modes for the dispersions have a direct impact on the coatings (different surface uniformities). The presence of weaker hydrophobic interactions promoting catalyst−ionomer and ionomer−ionomer interactions is supported for the inks prepared by using the D1st-Water and D-Premixed dispersions. Furthermore, the worsening of coatings for higher I/C ratio with D1st-Water and D-Premixed inks also support the presence of nonoptimal interactions, since more ionomer saturation did not lead to enhancements. These resulted in highly cracked structures upon drying, which, with the brightness adjustment, are more pronounced. The original images can be found in Figure S1. Moreover, the slightly better coating qualities for D-Premixed inks compared with D1st-Water inks also support the presence of anisotropic effects in the D-Premixed dispersion due to localized hydrophobic and ionic clusters.

With cross-sectional SEM of the resulting MEAs, the inhomogeneities are also visualized in some areas of the images, marked by light red circles in Figure 8. However, regardless of the dispersion preparation method, electrode

https://doi.org/10.1021/acsaem.5c00850
ACS Appl. Energy Mater. 2025, 8, 9256−9267

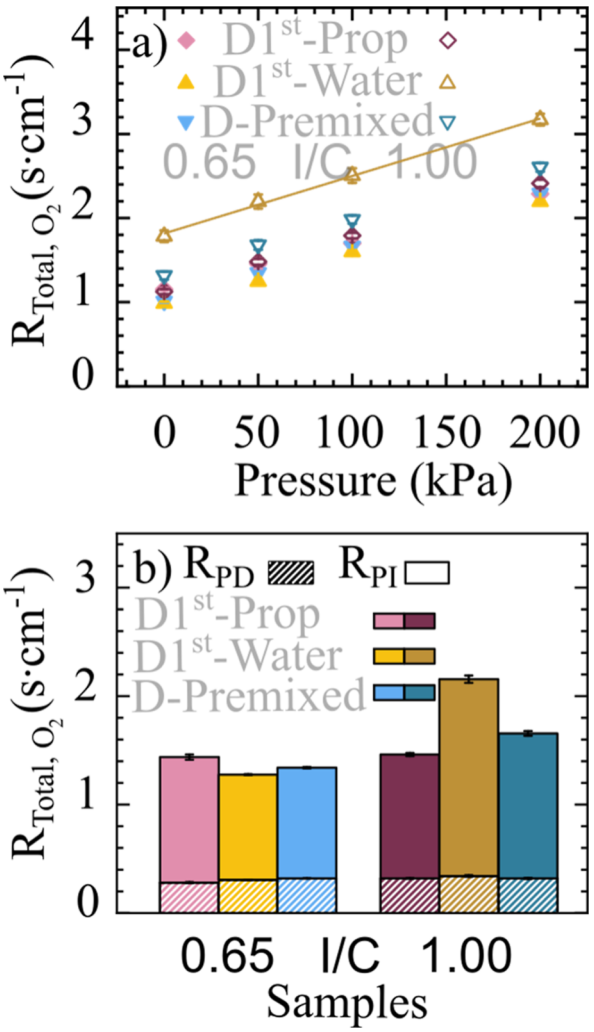

Figure 12. Mass transport properties of the different samples at 30% RH and 80 °C, with (a) showing the calculated total mass transport resistances at different pressures with a linear fit for I/C 0.65 D1st-Water (yellow —) and (b) showing the contribution of the pressure dependent and pressure independent components at 50 kPa gauge to the total resistance of I/C 0.65 D1st-Prop (pink −♦−), D1st-Water (yellow −▲−), and D-Premixed (blue −▼−) and 1.00 D1st-Prop (brown −◊−), D1st-Water (dark yellow −△−), and D-Premixed (teal −▽−).

thicknesses based on at least 15 measurements per electrode are found to be similar for the same I/C ratio. This also resulted in similar calculated void volume fractions for the different samples within the same I/C ratio (Table S1). As expected, lower void volume fractions were found for the I/Cs of 1.00 compared with the I/Cs of 0.65.

Electrochemical Testing. Figure 9 shows the polarization curves and HFRs of the differently prepared MEAs, measured at different relative humidities. Similar values are found for the HFRs among the samples, indicating little membrane contribution to performance differences. For the I/C ratio of 0.65 (Figure 9a−c), negligible differences are observed among the samples when tested at different RH. This suggests that for a low I/C ratio, the impacts of the different dispersions do not strongly affect fuel cell performance despite coating homogeneity variances due to differences in DLS, rheological, and wetting properties. For the I/C ratio of 1.00, however, clear differences are observed (Figure 9d−f). The I/C 1.00 D1st-Prop (brown −◊−) showed the best performance compared with D1st-Water (dark yellow −△−) and D-Premixed (teal −▽−) regardless of the RH. Moreover, the highly inhomogeneous coating I/C 1.00 D1st-Water (dark yellow −△−) showed the worst performance, 19−28% lower in peak power compared with 1.00 D1st-Prop (brown −◊−) and 18−19% lower compared with D-Premixed (teal −▽−). The higher ionomer concentration in the inks likely enabled better visualization of the impact of the dispersion. From the coatings, one notices that the inhomogeneities increase for high I/C ratios for D-Premixed and D1st-Water. The larger radii for D-Premixed and D1st-Water measured with DLS can in theory form rougher films with less uniformity and more microscale voids and cracks. The worse wetting properties of D1st-Water adds to this effect, which in turn results in a highly inhomogeneous coatings, with nonoptimal catalyst−ionomer interfaces and pore structures. Consequently, the performance can decrease at high current densities, where interfaces and structures become critical for mass transport.

Figure 10a,b display the Tafel slopes corrected for internal resistances and the ECSAs, respectively. Currents up to 100 mA cm^{-2} were included for the Tafel analysis, yielding Tafel slopes around ≈0.70 ± 0.03 mV dec^{-1}. The ECSAs were also in a similar range of ≈58.0 ± 2.0 m^2 g_{pt}^{-1}. These suggest that the different performances cannot be traced back to kinetic or activity differences.

The protonic sheet resistances and conductivity values of the CLs are displayed in Figure 11a,b. The protonic sheet resistances increase, and the conductivities decrease, for lower relative humidities and for a lower I/C ratio. For a given I/C ratio and RH, the proton transfer properties of the CLs are within a similar range and are not strongly affected by the ionomer dispersion type. Interestingly, the I/C 0.65 D1st-Water (yellow —) shows slight better values compared with I/C 0.65 D1st-Prop (pink —) and D-Premixed (blue —), despite the inhomogeneous coating quality, as shown in Figure 7. However, the protonic sheet resistance for I/C 1.00 D1st-Water (dark yellow —) was not better compared to the other samples. This suggests that the differences in proton conductivity are not directly due to the rheological, DLS, or contact angle differences of the dispersions and inks but rather likely a minor consequence of the coating inhomogeneity. For example, better mass transport properties for I/C 0.65 D1st-Water (yellow —) could have aided in the CL humidification during operation and ultimately in proton conduction. Furthermore, the results also suggest that the differences in the polarization curves for the high I/C ratios (Figure 9d−f) are due to a phenomenon different from proton conduction.

Mass transport resistances are displayed in Figure 12a,b. The deconvolution into pressure dependent, R_{PD,O_2}, and pressure independent, R_{PI,O_2}, resistance was done at a 50 kPa gauge backpressure, as this reflects the testing conditions. Figure 12a shows lower mass transport resistances for the MEAs with an I/C ratio of 0.65 compared with I/Cs 1.00, as expected. For I/Cs 0.65, R_{T,O_2} is found to be similar among the samples for all pressures, with the inhomogeneous D1st-Water (yellow −▲−) having arguably the lowest resistance. This in turn can explain the slightly better proton conduction properties in Figure 11. However, for I/Cs of 1.00, worse coating qualities showed considerably higher mass transport resistance behavior, with I/C 1.00 D1st-Water (dark yellow −△−) showing the highest, followed by I/C 1.00 D-Premixed (teal −▽−). On

https://doi.org/10.1021/acsaem.5c00850
ACS Appl. Energy Mater. 2025, 8, 9256−9267

the other hand, I/C 1.00 D1st-Prop (brown −◇−) had comparable resistances with I/Cs 0.65, being only slightly higher.

By deconvoluting the total mass transport resistances into pressure dependent and pressure independent components in Figure 12b, I/C 1.00 D1st-Water (dark yellow −△−) is found to have the highest pressure independent resistance. The higher R_{PI,O_2} suggests worse Knudsen diffusion processes in the CL and local O_2 diffusion through ionomer films.[26,34,35] These ultimately resulted in considerable performance differences in Figure 9d−f. Ultimately, the significantly poor coating quality, manifested by big aggregates from DLS, poor viscoelastic strengths from rheology, and poor wetting from contact angle measurements, led to poor interfaces and pore structures and therewith higher mass transport resistances.

CONCLUSION

Despite numerous available studies on ionomer dispersions and catalyst inks, few studies exist on the connection between them and how these ultimately impact fuel cell performance. In this study, we performed a solvent sequence addition variation for the preparation of 20 wt % ionomer dispersions while maintaining the same overall composition. Adding 1-propanol to the ionomer first (D1st-Prop) was shown to result in a more entangled polymer network with a higher viscosity, while inks prepared with this dispersion also showed better degrees of mixing. Ultimately, this led to the formation of more homogeneous CLs, which for the higher I/C ratio of 1.0 showed better electrochemical properties. On the other hand, adding water first to the ionomer (D1st-Water) resulted in less connected dispersions and lower viscosities. This also resulted in weaker hydrophobic interactions in inks, leading to inadequate mixing and nonoptimal film formation during coating. For the high I/C ratio, the worse coating qualities resulted in the lowest performances due to higher resistances for Knudsen diffusion in the CL and/or local O_2 diffusion through ionomer films. Premixing the solvents followed by ionomer addition (D-Premixed) caused combined effects. The coatings showed intermediate qualities, and the performance at the higher I/C ratio was also intermediate.

ASSOCIATED CONTENT

Supporting Information

The Supporting Information is available free of charge at https://pubs.acs.org/doi/10.1021/acsaem.5c00850.

Parameters used for void volume fraction calculation, along with the calculated values, electrode thicknesses, and catalyst loadings; original images of the electrodes taken with the Canon camera; representative fit for the protonic sheet resistance measurement; limiting current experiment response; and intensity distribution functions and autocorrelation functions for the DLS measurements for the inks and dispersions (PDF)

AUTHOR INFORMATION

Corresponding Author

Matthew Brodt − *Helmholtz Institute Erlangen-Nürnberg for Renewable Energy (IET-2), Forschungszentrum Juelich GmbH, Erlangen 91058, Germany;* orcid.org/0000-0002-6895-9889; Email: ma.brodt@fz-juelich.de

Authors

Marc Ayoub − *Helmholtz Institute Erlangen-Nürnberg for Renewable Energy (IET-2), Forschungszentrum Juelich GmbH, Erlangen 91058, Germany; Department of Chemical and Biological Engineering, Friedrich Alexander University Erlangen-Nürnberg, Erlangen 91058, Germany;* orcid.org/0009-0001-9977-254X

Maximilian Wagner − *Helmholtz Institute Erlangen-Nürnberg for Renewable Energy (IET-2), Forschungszentrum Juelich GmbH, Erlangen 91058, Germany;* Present Address: Fraunhofer-Institut für Keramische Technologien und Systeme (IKTS), Korrelative SpektroskopieCorrelative Spectroscopy, Äussere Nürnberger Strasse 62, 91301 Forchheim, Germany

Krishnaveni Anjala − *Department of Chemistry and Pharmacy & Interdisciplinary Center for Molecular Materials and Bavarian Polymer Institute, Friedrich Alexander University Erlangen-Nürnberg, Erlangen 91058, Germany*

Franziska Gröhn − *Department of Chemistry and Pharmacy & Interdisciplinary Center for Molecular Materials and Bavarian Polymer Institute, Friedrich Alexander University Erlangen-Nürnberg, Erlangen 91058, Germany;* orcid.org/0000-0003-1016-2583

Silke Christiansen − *Fraunhofer-Institut für Keramische Technologien und Systeme (IKTS), Korrelative Spektroskopie|Correlative Spectroscopy, Forchheim 91301, Germany*

Jochen Kerres − *Helmholtz Institute Erlangen-Nürnberg for Renewable Energy (IET-2), Forschungszentrum Juelich GmbH, Erlangen 91058, Germany; Chemical Resource Beneficiation Faculty of Natural Sciences, North-West University, Potchefstroom 2520, South Africa;* orcid.org/0000-0003-4972-6307

Simon Thiele − *Helmholtz Institute Erlangen-Nürnberg for Renewable Energy (IET-2), Forschungszentrum Juelich GmbH, Erlangen 91058, Germany; Department of Chemical and Biological Engineering, Friedrich Alexander University Erlangen-Nürnberg, Erlangen 91058, Germany;* orcid.org/0000-0002-4248-2752

Complete contact information is available at: https://pubs.acs.org/10.1021/acsaem.5c00850

Author Contributions

M.A.: conceptualization, methodology, resources, investigation, data curation, visualization, project administration, writing—original draft, review and editing. M.W.: conceptualization, methodology, resources, investigation, data curation, project administration, writing—review and editing. K.A.: investigation, writing—review. F.G.: resources, supervision, project administration, writing—review and editing. S.C.: supervision, project administration, writing—review. J.K.: resources, supervision, project administration, writing—review and editing. S.T.: conceptualization, methodology, resources, investigation, supervision, project administration, writing—review and editing, funding acquisition. M.B.: conceptualization, methodology, resources, investigation, supervision, project administration, writing—review and editing.

Notes

The authors declare no competing financial interest.

https://doi.org/10.1021/acsaem.5c00850
ACS Appl. Energy Mater. 2025, 8, 9256−9267

■ ACKNOWLEDGMENTS

Special thanks to Manuel Daum from the Department of Materials Science and Engineering, Materials for Electronics and Energy Technology, for demonstrating the setup used for capturing images. We thank Jakob Katsman for helping with the OAS measurements. We also would like to thank 3M for providing us with the ionomer granules.

■ REFERENCES

(1) Berlinger, S. A.; Dudenas, P. J.; Bird, A.; Chen, X.; Freychet, G.; McCloskey, B. D.; Kusoglu, A.; Weber, A. Z. Impact of Dispersion Solvent on Ionomer Thin Films and Membranes. *ACS Appl. Polym. Mater.* **2020**, *2* (12), 5824−5834.
(2) Gebel, G.; Loppinet, B. Colloidal structure of ionomer solutions in polar solvents. *J. Mol. Struct.* **1996**, *383* (1−3), 43−49.
(3) Loppinet, B.; Gebel, G.; Williams, C. E. Small-Angle Scattering Study of Perfluorosulfonated Ionomer Solutions. *J. Phys. Chem. B* **1997**, *101* (10), 1884−1892.
(4) Loppinet, B.; Gebel, G. Rodlike Colloidal Structure of Short Pendant Chain Perfluorinated Ionomer Solutions. *Langmuir* **1998**, *14* (8), 1977−1983.
(5) Yamaguchi, M.; Matsunaga, T.; Amemiya, K.; Ohira, A.; Hasegawa, N.; Shinohara, K.; Ando, M.; Yoshida, T. Dispersion of Rod-like Particles of Nafion in Salt-Free Water/1-Propanol and Water/Ethanol Solutions. *J. Phys. Chem. B* **2014**, *118* (51), 14922−14928.
(6) Aldebert, P.; Dreyfus, B.; Gebel, G.; Nakamura, N.; Pineri, M.; Volino, F. Rod like micellar structures in perfluorinated ionomer solutions. *J. Physiol. (Paris)* **1988**, *49* (12), 2101−2109.
(7) Moore, R. B.; Martin, C. R. Chemical and morphological properties of solution-cast perfluorosulfonate ionomers. *Macromolecules* **1988**, *21* (5), 1334−1339.
(8) Welch, C.; Labouriau, A.; Hjelm, R.; Orler, B.; Johnston, C.; Kim, Y. S. Nafion in Dilute Solvent Systems: Dispersion or Solution? *ACS Macro Lett.* **2012**, *1* (12), 1403−1407.
(9) Ngo, T. T.; Yu, T. L.; Lin, H.-L. Influence of the composition of isopropyl alcohol/water mixture solvents in catalyst ink solutions on proton exchange membrane fuel cell performance. *J. Power Sources* **2013**, *225*, 293−303.
(10) Kuo, A.-T.; Urata, S.; Nakabayashi, K.; Watabe, H.; Honmura, S. Coarse-Grained Molecular Dynamics Simulation of Perfluorosulfonic Acid Polymer in Water−Ethanol Mixtures. *Macromolecules* **2021**, *54* (2), 609−620.
(11) Mabuchi, T.; Huang, S.-F.; Tokumasu, T. Dispersion of Nafion Ionomer Aggregates in 1-Propanol/Water Solutions: Effects of Ionomer Concentration, Alcohol Content, and Salt Addition. *Macromolecules* **2020**, *53* (9), 3273−3283.
(12) Tarokh, A.; Karan, K.; Ponnurangam, S. Atomistic MD Study of Nafion Dispersions: Role of Solvent and Counterion in the Aggregate Structure, Ionic Clustering, and Acid Dissociation. *Macromolecules* **2020**, *53* (1), 288−301.
(13) Kusoglu, A.; Weber, A. Z. New Insights into Perfluorinated Sulfonic-Acid Ionomers. *Chem. Rev.* **2017**, *117* (3), 987−1104.
(14) Michelarakis, N.; Franz, F.; Gkagkas, K.; Gräter, F. Longitudinal strand ordering leads to shear thinning in Nafion. *Phys. Chem. Chem. Phys.* **2021**, *23* (45), 25901−25910.
(15) Khandavalli, S.; Iyer, R.; Park, J. H.; Myers, D. J.; Neyerlin, K. C.; Ulsh, M.; Mauger, S. A. Effect of Dispersion Medium Composition and Ionomer Concentration on the Microstructure and Rheology of Fe-N-C Platinum Group Metal-free Catalyst Inks for Polymer Electrolyte Membrane Fuel Cells. *Langmuir* **2020**, *36* (41), 12247−12260.
(16) Hoffmann, E.; Fischer, D.; Thoma, M.; Damm, C.; Lobaz, V.; Zhigunov, A.; Peukert, W. Impact of DAA/water composition on PFSA ionomer conformation. *J. Colloid Interface Sci.* **2021**, *582* (Pt B), 883−893.
(17) Novy, M. H. L. *Structure-Morphology-Property Relationships in Perfluorosulfonic Acid Ionomer Dispersions, Membranes, and Thin Films to Advance Hydrogen Fuel Cell Applications*; Virginia Tech, 2022.
(18) Yang, D.; Guo, Y.; Tang, H.; Wang, Y.; Yang, D.; Ming, P.; Zhang, C.; Li, B.; Zhu, S. Influence of the dispersion state of ionomer on the dispersion of catalyst ink and the construction of catalyst layer. *Int. J. Hydrogen Energy* **2021**, *46* (66), 33300−33313.
(19) Ayoub, M.; Freiberg, A. T. S.; Böhm, T.; Körner, A.; Hutzler, A.; Thiele, S.; Brodt, M. Continuous Graded Catalyst Layers for PEM Fuel Cells with Improved Humidity Range Tolerance. *J. Electrochem. Soc.* **2024**, *171* (11), 114503.
(20) Zhang, J.; Zhang, H.; Wu, J.; Zhang, J. Chapter 3 - Techniques for PEM Fuel Cell Testing and Diagnosis. In *Pem Fuel Cell Testing and Diagnosis*; Zhang, J., Zhang, H., Wu, J., Zhang, J., Eds.; Elsevier, 2013; pp 81−119.
(21) *PEM Fuel Cell Diagnostic Tools:Linear Sweep Voltammetry; PEM fuel cell durability handbook*; Wang, H., Yuan, X.-Z., Li, H., Eds.; CRC Press, 2011.
(22) Murthy, M., Sisofo, N. T., Baczkowki, C. A. Method and device to improve operation of a fuel cell. WO 2006081009 A2, 2006.
(23) Liu, Y.; Murphy, M. W.; Baker, D. R.; Gu, W.; Ji, C.; Jorne, J.; Gasteiger, H. A. Proton Conduction and Oxygen Reduction Kinetics in PEM Fuel Cell Cathodes: Effects of Ionomer-to-Carbon Ratio and Relative Humidity. *J. Electrochem. Soc.* **2009**, *156* (8), B970.
(24) Neyerlin, K. C.; Gu, W.; Jorne, J.; Clark, A.; Gasteiger, H. A. Cathode Catalyst Utilization for the ORR in a PEMFC. *J. Electrochem. Soc.* **2007**, *154* (2), B279.
(25) Harzer, G. S. Boosting High Current Density Performance of Durable, Low Pt-Loaded PEM Fuel Cells. Dissertation,Technische Universität München, 2018 https://mediatum.ub.tum.de/1449542.
(26) Baker, D. R.; Caulk, D. A.; Neyerlin, K. C.; Murphy, M. W. Measurement of Oxygen Transport Resistance in PEM Fuel Cells by Limiting Current Methods. *J. Electrochem. Soc.* **2009**, *156* (9), B991.
(27) Roney, A. B.; Space, B.; Castner, E. W.; Napoleon, R. L.; Moore, P. B. A Molecular Dynamics Study of Aggregation Phenomena in Aqueous n -Propanol. *J. Phys. Chem. B* **2004**, *108* (22), 7389−7401.
(28) Yi, Y. D.; Bae, Y. C. Swelling behaviors of proton exchange membranes in alcohols. *Polym. J.* **2017**, *130*, 112−123.
(29) Allahyarov, E.; Taylor, P. L. Role of electrostatic forces in cluster formation in a dry ionomer. *J. Chem. Phys.* **2007**, *127* (15), 154901.
(30) Aldebert, P.; Dreyfus, B.; Pineri, M. Small-angle neutron scattering of perfluorosulfonated ionomers in solution. *Macromolecules* **1986**, *19* (10), 2651−2653.
(31) Szajdzinska-Pietek, E.; Schlick, S.; Plonka, A. Self-Assembling of Perfluorinated Polymeric Surfactants in Nonaqueous Solvents. Electron Spin Resonance Spectra of Nitroxide Spin Probes in Nafion Solutions and Swollen Membranes. *LANGMUIR* **1994**, *10* (7), 2188−2196.
(32) Mehrazi, S.; Homayouni, T.; Kakati, N.; Sarker, M.; Rolfe, P.; Chuang, P.-Y. A. A Rheo-Impedance investigation on the interparticle interactions in the catalyst ink and its impact on electrode network formation in a proton exchange membrane fuel cell. *Appl. Energy* **2024**, *359*, 122680.
(33) Mashio, T.; Ohma, A.; Tokumasu, T. Molecular Dynamics Study of Ionomer Adsorption at a Carbon Surface in Catalyst Ink. *Electrochim. Acta* **2016**, *202*, 14−23.
(34) Nonoyama, N.; Okazaki, S.; Weber, A. Z.; Ikogi, Y.; Yoshida, T. Analysis of Oxygen-Transport Diffusion Resistance in Proton-Exchange-Membrane Fuel Cells. *J. Electrochem. Soc.* **2011**, *158* (4), B416.
(35) Della Bella, R. K. F.; Stühmeier, B. M.; Gasteiger, H. A. Universal Correlation between Cathode Roughness Factor and H 2/Air Performance Losses in Voltage Cycling-Based Accelerated Stress Tests. *J. Electrochem. Soc.* **2022**, *169* (4), 044528.

https://doi.org/10.1021/acsaem.5c00850
ACS Appl. Energy Mater. 2025, 8, 9256−9267